Formation and Spreading of Antarctic Deep and Bottom Waters Inferred from a Chlorofluorocarbon (CFC) Simulation

Christian B. Rodehacke [*]   Hartmut H. Hellmer [†]   Oliver Huhn [‡]

Aike Beckmann [§]

April 25, 2007

Abstract

The formation of deep and bottom waters along Antarctica's perimeter is determined by ocean interaction with the atmosphere, sea ice, ice shelves, and bottom topography. It initiates a chain of processes that contribute to the ventilation of the global abyss. To identify the formation sites and investigate the combined effects of the local forcing mechanisms on water mass transformation and spreading in the Southern Ocean, chlorofluorocarbon (CFC) simulations with the regional ocean circulation model (BRIOS-1) were performed. The model uses terrain-following vertical coordinates to better represent both near-bottom and mixed layer processes, and includes an explicit formulation of the ice shelf-ocean interaction. In agreement with observations, the results show the main deep and bottom water formations sites to be located in the Ross Sea, Prydz Bay, and southwestern Weddell Sea. The Ross Sea ventilates the South East Pacific and Australian Antarctic Basins. Both Ross Sea and Prydz Bay ventilate via the Antarctic Coastal Current the Weddell-Enderby Basin. The latter signal is overprinted by sources in the Weddell Sea which ventilate the South Scotia Sea and also the Weddell-Enderby Basin. Despite the general agreement between observed and simulated quantities like bottom layer CFC distribution and inventories along the Greenwich Meridian, the model tends to underestimate the ventilation of the abyssal ocean like other models with coarse resolution.

[*]University Bremen, Germany, *Present address:* Department of Applied Physics and Applied Mathematics, Columbia University, Armstrong Hall, 2880 Broadway, New York, NY 10025, USA

[†]Alfred-Wegener-Institute for Polar and Marine Research, Germany

[‡]University Bremen, Germany

[§]Alfred-Wegener-Institute for Polar and Marine Research, Germany *Present address:* University of Helsinki, Finland

1 Introduction

In the Southern Ocean deep and bottom waters are formed at the rim of broad continental shelves (e.g. Baines and Condie (1998)), which are fringed by large ice shelves. The four major contributing areas are located in the southwestern/western Weddell Sea near Filchner-Ronne/Larsen Ice Shelf, the Ross Sea in front of Ross Ice Shelf, Prydz Bay off Amery Ice Shelf, and the Adélie coast region at the transition between the Pacific Ocean and Indian Ocean (for locations see Fig. 8). Here, water mass formation is controlled by ocean interaction with ice shelves and with the atmosphere resulting in growth and decay of the mainly seasonal sea ice cover, and the mixing of water masses of different characteristics and origin. The two processes, identified to form deep and bottom waters, include the mixing of Modified Circumpolar Deep Water (MCDW) with:

- High Salinity Shelf Water (HSSW), which results from brine release during sea ice formation on the continental shelf (Foster and Carmack, 1976, 1977),

- Ice Shelf Water (ISW), which originates from the modification of HSSW at ice shelf bases and thus carries the glacial meltwater signal (Foldvik et al., 1985a,b).

The mixing products descend along the continental slope while entraining ambient lighter water masses. Depending on the entrainment rate, the final water mass stabilizes at different depths to become either deep (e.g. Weddell Sea Deep Water, WSDW) or bottom water (e.g. Weddell Sea Bottom Water, WSBW).

During contact with the atmosphere, the ocean exchanges gases like the anthropogenic chlorofluorocarbons (CFC) which leads to increased concentrations in the surface layer. As a result of enhanced sea ice formation on the continental shelf, deep convection homogenizes the water column, i.e., transports CFCs downward. The CFC signatures are transferred to the abyssal ocean as newly formed dense water masses descend along the continental slope.

To investigate the role of the Southern Ocean and, in particular, of the Weddell Sea in the ventilation of the deep ocean, a realistic CFC input was added to a regional ocean circulation model for the Antarctic marginal seas including the major ice shelf caverns (BRIOS 1.0, Beckmann et al. (1999)). Rodehacke et al. (006a) analyzed the spreading of deep and bottom waters carrying the ISW signal based on steady state tracers, the noble gases helium and neon. In this study the integral effect of both formation processes is considered using transient tracers with time-dependent input functions.

The paper is structured as follows: Section 2 describes the model and the tracer implementation. Validation of the CFC input (Section 3) is followed by the inspection of the horizontal spreading paths of freshly ventilated water masses (Section 4) and the comparison of the results with observations along two sections (Section 5) which cross both Weddell Gyre cells. The investigation of the vertical CFC distribution focuses on the penetration depth and the model's ability to simulate deep cores of elevated tracer concentrations (Section 6). For a quantitative comparison, modeled and observed inventories are calculated along the Greenwich Meridian. In Section 7, the modeled flow of deep and bottom waters into the Scotia Sea is used to explore the spreading

paths beyond the Weddell Sea and to validate the results. The paper concludes with a summary.

2 The model

The regional ocean circulation model BRIOS-1 is a modified version of the s-coordinate primitive equation model SPEM (Haidvogel et al., 1991; Beckmann et al., 1999). It comprises the circumpolar ocean between $50°$S and $82°$S with a higher resolution of $1.5° \times 1.5° \cos\phi$ in the Atlantic Sector. Outside of the Atlantic, zonal grid spacing increases gradually to $6.75° \times 1.5° \cos\phi$ (Fig. 1 in Beckmann et al. (1999)). More details of the physical model are provided in Beckmann et al. (1999).
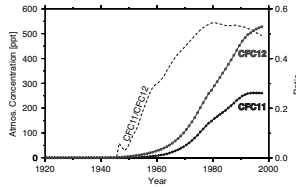

Figure 1: Atmospheric CFC concentration histories in the southern hemisphere (after Walker et al. (2000)).

The model is initialized using data from the Hydrographic Atlas of the Southern Ocean (Olbers et al., 1992). It is forced using a climatological year, derived from the stand-alone sea ice-mixed layer model BRIOS-0, which in turn was driven with ECMWF re-analysis data for the period 1985–97. The model was integrated for 20 years to reach a quasi-stationary state (Beckmann et al., 1999). From this state the tracer simulation started in CFC-year 1940 with atmospheric CFC11 and CFC12 concentrations of 0 ppt and 0.3 ppt, respectively. This is when atmospheric concentrations (Fig. 1) of both CFCs began to increase exponentially (Walker et al., 2000) and before both CFCs contributed significantly to the CFC water column inventories.

2.1 Tracer boundary condition

The tracer input at the atmosphere-ocean interface is implemented as a flux boundary condition according to Wanninkhof (1992) and Asher and Wanninkhof (1998), assuming that the flux of slightly soluble, non-reactive gases depends on the concentration gradient at the interface. Since stronger winds enhance turbulent mixing in the upper mixed layer, which leads to an increased gas flux, the wind influence is considered by using a computed climatology of squared winds ($u_{10\ \mathrm{m}}^2$). In contrast, a sea ice cover can significantly reduce the air-sea fluxes. Therefore, according to England et al. (1994), the boundary condition includes the flux reduction by the grid box fraction covered by sea ice (A). The complete formulation of the gas exchange is:

$$F_G = k_0(\alpha_s p_{\mathrm{atmos}} - c_w)(1 - A)\frac{u_{10\ \mathrm{m}}^2}{\sqrt{\mathrm{Sc}}}, \tag{1}$$

3

where k_0 is the piston velocity — derived from bomb produced radiocarbon invasion rates into the ocean and, hence, includes implicitly the Schmidt number for ^{14}C (England et al., 1994), c_w the surface concentration, and p_{atmos} represents the temporal evolution of the atmospheric CFC concentration (Walker et al., 2000) which is assumed to be spatially constant. We presume a mean atmospheric total pressure of 0.98 atm (992.94 hPa), use the solubilities $\alpha_s(\Theta, S)$ of Warner and Weiss (1985), and the description of the Schmidt number (Sc) according to Zheng et al. (1998). The sea ice concentration A, as part of the forcing fields — a climatological year based on the above mentioned re-analysis data from 1985 to 1997 — agrees well with satellite-derived sea ice concentrations (R. Timmermann, pers. comm.).

Within the northern relaxation zone of the model subsurface CFC concentrations are nudged towards zero because for water masses flowing from the Antarctic Circumpolar Current (ACC) to the deep and bottom water formation sites one can assume the CFC concentrations to be negligible. For example, in 1990 CFC concentrations in Drake Passage for depths greater than $\sigma_2 = 38.8$ were below the detection limit of 0.01 pmol/kg (Roether et al., 1993).
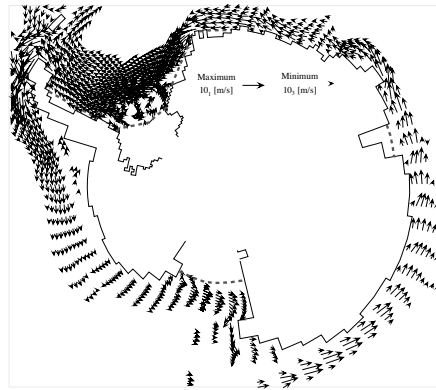
3 Validation

Figure 2: Velocity vectors in the bottom layer at Antarctica's perimeter (model year 60). For better visualization, small and large values are omitted. Ice shelve edges are marked by dashed lines.

The validation of the dynamical model setup is described by Beckmann et al. (1999) and is recapitulated here. The flow field (Fig. 2), described by the streamfunction (Fig. 3), reproduces the known circulation features: the eastward flowing ACC, the cyclonic (clock-wise rotating) Weddell, Ross and Kerguelen Gyres as well as the Antarctic Coastal Current flowing westward close to the Antarctic margin. Transports across two sections compare well with reported rates across the Greenwich Meridian of 60±10 Sv (Schröder and Fahrbach, 1999) and across the Joinville Island-Cap Norvegia section of 30±10 Sv (Fahrbach et al., 1994) (sections follow the green lines in Figure 3). The
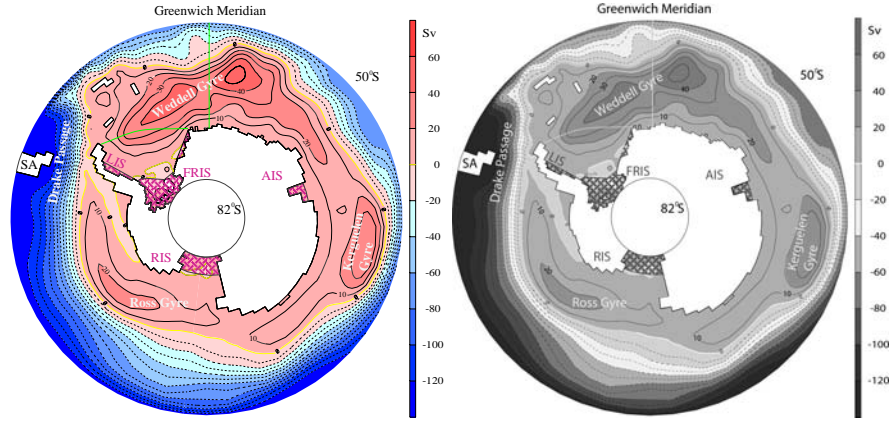
Figure 3: Annual mean of the streamfunction of model year 60 in Sverdrup (1 Sv =$10^6 \frac{m^3}{s}$). Model results are compared with observations along sections indicated as green lines. Considered ice shelves are (hatched in red): Filchner-Ronne Ice Shelf (FRIS), Ross Ice Shelf (RIS), Amery Ice Shelf (AIS), and Larsen Ice Shelf (LIS). SA is South America.

simulated annual mean fields of temperature and salinity (Fig. 9a and 9b in (Beckmann et al., 1999)) along the Joinville Island-Cap Norvegia section reproduces well the observed doming (Fig. 7a and 7b in Fahrbach et al. (1994)). The simulated bottom temperatures are slightly too warm, which might be related to an insufficient transport of freshly ventilated water masses into the depth (as we will show later). The salinity agrees well but the subsurface maximum is too large in horizontal and vertical extent.

A unique feature of this model is the integration of major ice shelf caverns including the ocean-shelf ice interaction. Each cavern has its own signature in the Θ-S-space as the Θ-S-diagram shows (Fig. 4). Furthermore, the caverns are a source of relatively cold and fresh water masses, which changes, in particular, the properties of the near-surface layers. These are distinctly fresher (up to -0.22) and cooler (up to $-1.5\,°C$) (Figures 13a and 13b in Beckmann et al. (1999)). Since the upper water column of the western Weddell Sea is stabilized by these lighter water masses, convection is reduced which preserves the warmer and saltier deep water masses. As the Θ-S-diagram shows, the model reproduces the linear mixing between ISW and WSDW, but the annual mean lacks HSSW (> 34.75) at the surface freezing point. On the continental shelf in front of Filchner-Ronne Ice Shelf (FRIS) observed and simulated hydrographic properties and helium saturations, which are strongly determined by the addition of glacial melt due to ocean–ice shelf interaction, indicate that the model reproduces the general hydrographical structure and the ISW outflow. Furthermore, the analysis highlights the importance of the ocean-ice shelf interaction but also suggests that model resolution might be too coarse to prevent warm and salty water masses from penetrating onto the continental shelf (Rodehacke et al., 006a). Nevertheless, a comprehensive treatment of the sub-ice shelf environment and the related freshwater fluxes seems to be important for an adequate representation of observed local and large-scale hydrographic condi-
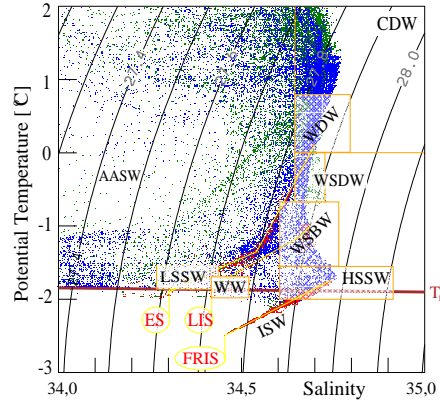
tions (Hellmer, 2004).

Figure 4: Annual mean of the temperature vs. salinity relation for model year 60. Red dots represent water masses within ice shelf caverns of the Weddell Sea with each cavern having its own Θ-S characteristic; FRIS: Filchner-Ronne Ice Shelf, LIS: Larsen Ice Shelf, and ES: Eastern Ice Shelves (Riiser-Larsen Ice Shelf Complex). The blue dots represent the Weddell Sea while green dots stand for the remaining grid boxes outside the Weddell Sea. The horizontal dark-red line depicts the surface freezing temperature T_f as a function of salinity. The hydrographic ranges of water masses are highlighted by yellow boxes; AASW: Antarctic Surface Water, CDW: Circumpolar Deep Water, HSSW: High Salinity Shelf Water, ISW: Ice Shelf Water, LSSW: Low Salinity Shelf Water, WDW: Warm Deep Water, WSBW: Weddell Sea Bottom Water, WSDW: Weddell Sea Deep Water, and WW: Winter Water.

3.1 CFC11 surface saturation

In this article we only present results for the tracer CFC11 because they are almost identical with those for CFC12, and our simulation covers the complete CFC11 history. The modeled CFC input into the ocean is validated by comparing observed and simulated CFC11 degrees of relative equilibrium with the atmosphere (saturations) in the surface mixed layer. For the validation only the saturation is assumed to be constant in time for the observation period (1990–1998), which is a common assumption due to the lack of observations to resolve seasonal to interanual variability. The simulation driven with an annual cycle shows a distinct annual cycle in the mixed layer CFC saturation which is discussed below (Fig. 7).

The compilation of CFC11 saturations of the upper 55 m in the water column (Fig. 5a) bases on observations which were measured during the period 1990–98. In general, the saturation decreases from north to south. East of the Greenwich Meridian (20 °E – 30°E) surface water with higher saturation penetrates southward. This coincides with the southward deflection of the ACC and defines the eastern boundary of the Weddell Gyre (e.g., Schröder and Fahrbach (1999)). The reduced saturation above Maud Rise
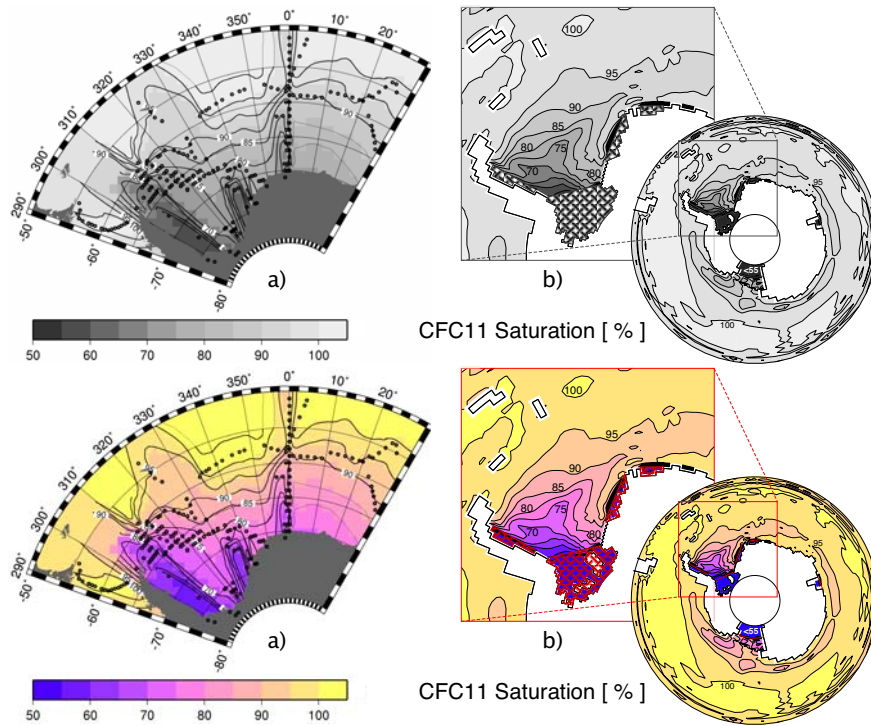
Figure 5: Observed a) and simulated b) CFC11 saturation in the ocean surface mixed layer. Observations in the Weddell Sea (dots) are based on cruises *ANT X/4*, *ANT XII/3*, *ANT XIII/3*, *ANT XV/4*, *JCR10*, *JCR40*, *M11*, WOCE-campaigns *S04I* and *S04p*, and values from *Ice Station Weddell* (Mensch et al., 2000). Simulated values represent the mean of the modeled CFC11 saturation fields at the time of the observations, which have a strong summer bias. The blow-up b) focuses on the Weddell Sea including its ice shelf caverns (hatched in red).

(Greenwich Meridian) is caused by topographically induced upwelling of less saturated deep waters (Rodehacke et al., 007b; Muench et al., 2001). Lowest values occur in the perennial ice-covered southwestern and western Weddell Sea, whereas off FRIS and in the central Weddell Sea single saturations range from 50% to almost 100%. In Drake Passage, however, single observations exceed the equilibrium saturation with values of up to 110%. This may be caused by warming of the surface mixed layer which decreases the equilibrium concentration before gas exchange can re-establish the equilibrium — Within the upper several tens of decimeters radiation heats instantaneously the ocean while matter has to travel from the atmosphere-ocean interface to an arbitrary point in the water column. In addition, molecular diffusion in the ocean skin layer controls the exchange rate which is two orders of magnitude higher for heat ($\mathcal{O}(10^{-7})$ m^2/s) than for matter ($\mathcal{O}(10^{-9})$ m^2/s). Judged from repeat measurements within profiles and at nearly the same time and location, the derived mean values have an uncertainty of 5%–10% for open ocean and 10%–20% for partially ice-covered seas. The temporal fluctuation (for the period 1990–98) at selected stations also reaches 10%, most likely related to the variations in sea ice extent (Gloersen et al., 1992).

The modeled CFC11 saturation (Fig. 5b) shows a small band around Antarctica with values below 95%. This is due to the slow retreat of the sea ice cover which has not completely disappeared by March/April (time of most of the observations). A tongue of higher-saturated water spreads from the Greenwich Meridian with the coastal current into the southern Weddell Sea (blow-up). In front of FRIS and Larsen Ice Shelf (LIS) the saturation drops below 60% because of the perennial sea ice cover. Lowest saturations ($< 55\%$) occur in the ice shelf caverns where the thick ice prevents a gas exchange with the atmosphere while mixing with less saturated shelf waters continues.

Since the variability of the simulated concentrations corresponds to observed fluctuations of the saturation, by considering that the solubility function ($\alpha_s(\Theta, S)$) is almost constant because temperature and salinity do not significantly change, the estimated uncertainty of the spatial saturation distribution is $\leq 10\%$ for the investigation period. Between 1990 and 1998 the simulated mean saturation increases in front of FRIS and in the Weddell Sea by 7.2% and 4%, respectively (Rodehacke et al., 007b). Therefore, the observed and simulated saturations are equal within the range of uncertainties. The relatively large observed uncertainty is caused by small scale processes and reflects interannual variations of environmental conditions which strongly influence the spatial saturation distribution.

If the CFC surface concentration and saturation were exclusively controlled by the gas flux across the atmosphere-ocean interface, we would obtain excellent agreement between observations and simulation, as the flux boundary condition and its driving parameters (here A, Θ, S, u^2, and p_{atmos}) would be comparable between observations and simulation. However, mass exchange between the mixed layer and deeper layers (mixed layer entrainment/detrainment) alters the mixed layer hydrography, tracer concentration, and saturation. The time scale ratio between mass exchange across the mixed layer base and the gas exchange through the atmosphere-ocean interface determines whether the entrainment/detrainment impacts the surface gas concentration. The entrainment/detrainment alters the surface concentration unless the gas exchange would be faster. Therefore, an adequate representation of the mixed layer subsurface interaction is essential for a realistic simulation of tracer concentrations and inventories

8

in deep and bottom waters (Doney and Jenkins, 1988). In particular, both the seasonal cycle of the mixed layer dynamics (Haine and Richards, 1995) and the sea ice concentration (Rodehacke et al., 007b) control surface concentrations and CFC fluxes between atmosphere and ocean.

The continental shelf area in front of FRIS is a vital deep and bottom water formation site in the Southern Ocean (Fig. 8) where the sea surface density is essentially controlled by the sea surface salinity (SSS). Here, these both parameters have the highest negative correlations (-0.94 (Rodehacke et al., 007b)) with the CFC11 flux (Fig. 6), because a lower/higher SSS is related to a lower/higher sea ice concentration (sea ice melting/formation), which allows a higher/lower CFC flux. The correlation between the CFC flux and the sea ice concentration is -0.75 (Rodehacke et al., 007b). In contrast, convection triggered by sea ice formation deepens the mixed layer, which entrains less saturated water and, ultimately, increases the flux driving concentration gradient between surface layer and atmosphere (Eq. 1). Since the flux reduction as a result of the sea ice cover overwhelms the enhanced concentration gradient, a deeper mixed layer causes a reduced CFC flux (correlation of CFC flux/mixed layer depth -0.66 (Rodehacke et al., 007b)). Due to the complex interplay between the temperature/salinity dependence of the equilibrium concentration, penetration of CFC-poor water masses onto the continental shelf, and a reduced gas flux due to sea ice coverage, sea surface temperature (SST) and salinity flux are not strongly correlated with the CFC flux (correlation 0.2 and 0.5, respectively (Rodehacke et al., 007b)).
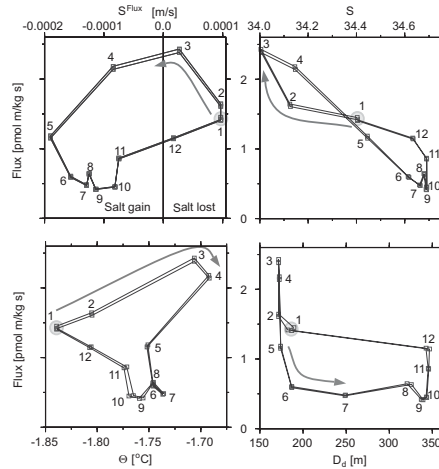

Figure 6: CFC11 flux across the atmosphere-ocean interface dependence against salt flux (S^{Flux}, negative values = salt gain in the surface due to sea ice formation), sea surface salinity (S, SSS), sea surface temperature (Θ, SST), mixed layer depth (D_d; defined as the layer, in which the density changes by 1%) for the model years 1998–2000. The numbers at the data points indicate the month and the arrows the direction of the temporal evolution.

To capture the seasonal variability of the simulated CFC11 saturation, we inspect
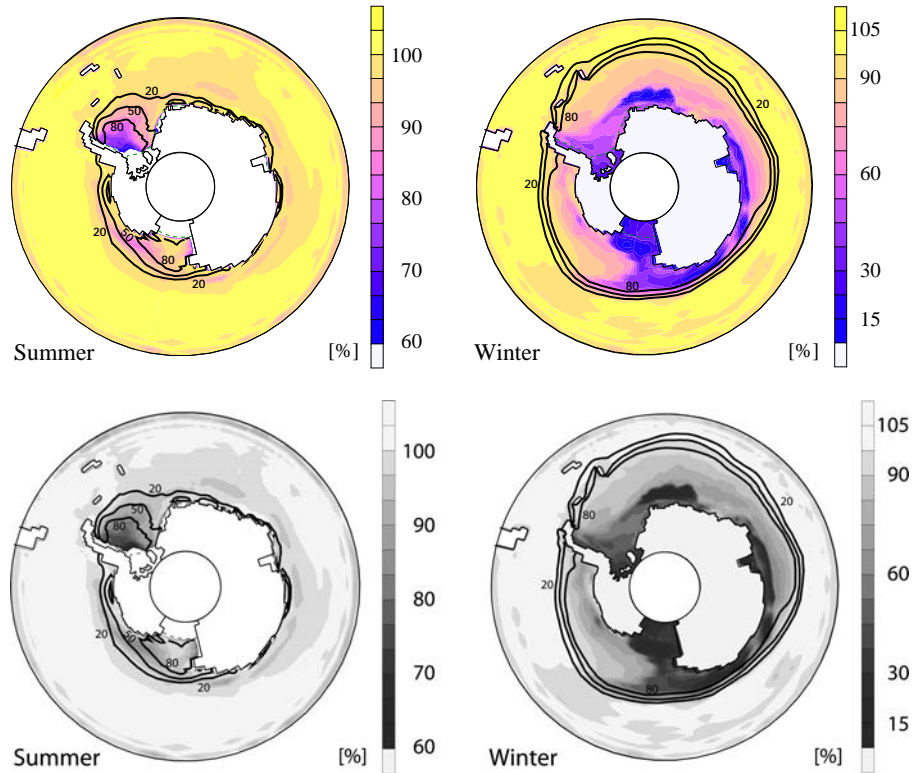
Figure 7: Simulated CFC11 surface saturations for the year 1998. The summer maximum (winter minimum) is based on saturations for March/April (October/November). Note the different color scale for both figures. The contour lines represent sea ice concentrations for March (summer) and October (winter) with intervals of 20%, 50%, and 80%. The ice shelf edges are depicted as green dashed lines.

its spatial distributions during the seasonal minimum and maximum (Fig. 7) for the year 1998. Maximum saturation, based on values of the summer months March and April, occurs in the ACC during March while further south it appears a month later. The retreating sea ice delays the onset of devaluated surface saturations. For all regions in the Southern Ocean covered by perennial sea ice the maximum CFC saturation lags two months behind the minimum sea ice concentration (Rodehacke et al., 007b). Maximum saturations range from 50% to 103% with lowest values in the Ross Gyre (85%) and in the western Weddell Sea (50%).

Minimum saturations (Fig. 7) occur at the end of winter in October and November. They appear at Antarctica's periphery where subsurface water masses rise to the surface while sea ice blocks the gas exchange. Extreme low saturations are found in the southwestern Weddell Sea and, in particular, in the coastal regions from the Ross Ice Shelf to the Indian Ocean and near Maud Rise where deep water masses are brought to shallower levels.

10

The pattern of maximum and minimum saturations around Antarctica is strongly controlled by the sea ice distribution. During summer the lowest saturations in the southern Weddell Sea are caused by persisting high sea ice concentrations, which suppress the gas flux over highly undersaturated water masses. During winter, the northernmost extent of the sea ice edge marks, like in the Ross Sea and eastern Indian Ocean, the northern boundary of low surface saturations. A detailed analysis of the seasonal and long-term evolution of the CFC11 and CFC12 saturations as well as the correlation between CFC fluxes and various parameters is given in Rodehacke et al. (007b).

4 Horizontal spreading structures

The simulated CFC11 concentrations in the bottom layer around Antarctica (Fig. 8) reveal three distinct regions of high values, the Ross Sea in front of the Ross Ice Shelf, Prydz Bay in front of Amery Ice Shelf, and the southwestern Weddell Sea where highest concentrations appear near Berkner Island. In addition, high values are also found along the coasts of Adélie Coast and Wilkes Land.

Freshly ventilated water masses from the Ross Sea continental shelf spread with the cyclonic Ross Gyre to split into two branches at Cape Adare. One follows the cyclonic circulation ventilating the Southeast Pacific Basin, while the other mixes into the Antarctic Coastal Current to advance toward the Indian Ocean.

High concentrations also exist in front of Adélie Coast and Wilkes Lands. On the short way from the formation sites to the continental shelf break, the freshly ventilated water masses mix with ambient water of the westward flowing coastal current. Due to a coarser resolution outside the Atlantic sector, the model fails to represent the observed tongue-like spreading (Orsi et al., 1999) of freshly ventilated water masses from the continental shelf off Adélie Land, an important source for the ventilation of the Australian-Antarctic Basin (**?**). A detailed analysis with artificial/numerical tracers (not shown) indicates that at greater depth the Kerguelen-Plateau blocks the westward spreading of freshly ventilated water masses. However, these waters flow northward and contribute to the ventilation of the Australian-Antarctic Basin. At the northern rim of Prydz Bay in front of Amery Ice Shelf additional CFC-containing water masses are mixed into the current. At the transition from the Indian Ocean to the Atlantic Ocean, marked by the Gunnerson and Astrid Ridges, the freshly ventilated water masses start to meander following f/h contours.

In the Weddell Sea more CFC-enriched shelf water, in particular that from the broad southern continental shelf including ISW from the FRIS cavern (Rodehacke et al., 006a), is added to the coastal current as it follows the continental shelf break towards the northern tip of the Antarctic Peninsula.

Here, the path splits into two branches of different depth. The shallow branch crosses the South Scotia Ridge to either spread eastward within the Weddell-Scotia Confluence or westward towards Drake Passage where, after passing, it contributes to the Antarctic Coastal Current. This current flows westward, hardly affected by the high-concentrated waters in the Bellingshausen Sea which apparently remain on the continental shelf, to provide a limited contribution to the ventilation of the deep ocean in the Southeast Pacific. By entering the eastern Ross Sea, the coastal current closes

the circumpolar transport of CFC enriched waters. The deeper branch at the tip of the Antarctic Peninsula flows eastward with the gyre circulation and continues to split while losing its CFC signature. Between the South Orkney and South Sandwich Islands, for example, it enters the Scotia Sea to become incorporated in the lower portion of the ACC. An examination of the simulated CFC outflow into the South Scotia Sea and beyond and a comparison with observations is given below (Section 7).
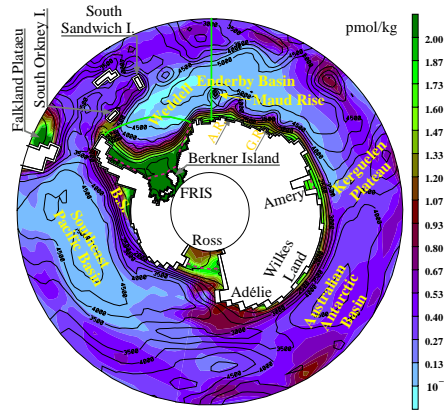

Figure 8: Simulated CFC11 concentration in the bottom layer in April 1998. The contour lines represent the bottom topography in 500 m intervals. The edges of ice shelves are depicted as red dashed lines, the green lines indicate the location of the Greenwich Meridian and Weddell Sea cross sections. The abbreviations are Bellingshausen Sea (B.S.), Astrid Ridge (A.R.), and Gunnerson Ridge (G.R.).

The high CFC concentration on the Falkland Plateau (Fig. 8) represents a subduction of water masses. However, it might be a model artifact due to the vicinity of the northern restoring zone. But, parts of the ACC leave the model domain in this area and CFC subsurface concentrations are nudged to zero at the northern boundary. Therefore, this feature might represent the subduction of either South Atlantic Mode Water or Antarctic Intermediate Water (Talley, 1996, 1999; Miranda et al., 1999).

5 Vertical CFC structure

In the following, the two repeatedly sampled sections shown in Fig. 8 crossing the central Weddell Sea and continuing along the Greenwich Meridian are addressed.

5.1 Weddell Sea cross section

Our interest is focused on the only completely sampled central Weddell Sea section of 1996 (*ANT XIII/4*). A detailed description of this and further sections in this area, covering the period from 1992 (*ANT X/4*) to 1998 (*ANT XV/4*), is provided by Hoppema et al. (2001).
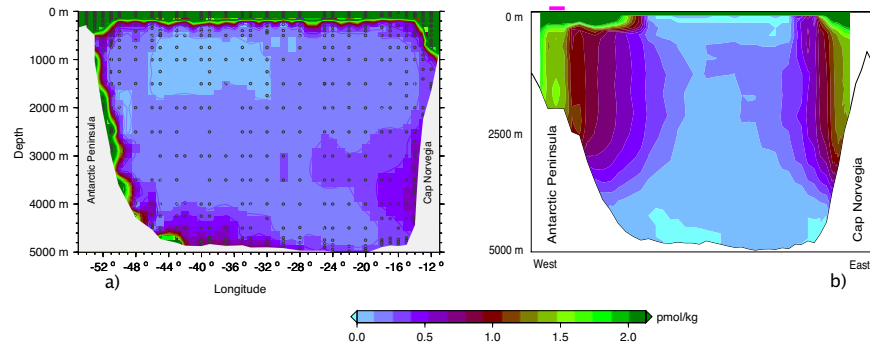
Figure 9: Vertical section of CFC11 concentration across the central Weddell Sea for 1996; a) observation from *ANT XIII/4* and b) simulation. The track is shown in figure 8.

Due to contact with the atmosphere, highest CFC concentrations are found in the surface mixed layer, separated by a strong gradient from the underlying water where concentrations gradually decrease with depth (Fig. 9a). Near the coast, water masses of the mixed layer descend to depths of 250 m (northwest) and 800 m (southeast), caused by wind-induced Ekman pumping (Fahrbach, 1993) while the upper water column is strongly stratified due to freshwater from sea ice melting. Characteristic features of this cross section are the extremely high concentrations at the entire continental slope off the Antarctic Peninsula and the core at 3500 m depth off Cap Norvegia. The former feature mainly results from newly formed deep and bottom waters triggered by deep convection on the southern (Carmack and Foster, 1975; Foster et al., 1987; Fahrbach et al., 1991) and western (Fahrbach et al., 1995; Weppernig et al., 1996; Gordon, 1998; Huhn et al., 2006) Weddell Sea continental shelf and consecutive sinking and spreading. The latter indicates ventilation of the deep ocean by an eastern (upstream) source (Hoppema et al., 2001; Schodlok et al., 2001; Klatt et al., 2002).

As observed, the highest concentrations occur in the model's surface mixed layer, which is separated from the water beneath by a sharp gradient that seems to be stronger than the non-continuous CFC observations suggest (Fig. 9b). Nevertheless, this gradient indicates an adequate parameterization of vertical mixing; the importance of this parameterization in seasonally ice-covered regions was emphasized by Timmermann and Beckmann (2004). At both continental slopes covered by the cross section, an extended layer of CFC-enriched water exists encompassing the surface mixed layer. Concentration as well as horizontal extension of these layers rapidly decrease with increasing depth within the upper 500 m. Below 500 m, concentrations slightly decrease but horizontal extension increases with depth for concentrations ≤ 0.5 pmol/kg. The simulated and observed eastern cores both have a concentration > 0.5 pmol/kg. However, the former is located at 1000 m instead of 3500 m as observed. This indicates the model's deficiency to transport freshly ventilated water masses to great depth.

At the western continental slope the observed concentration at 2250 m depth ex-

13

ceeds 2 pmol/kg, while the simulated one is only 1 pmol/kg. This discrepancy might be due to a larger horizontal extension of modeled high concentrations. In addition, in a narrow region (magenta colored line on top of Fig. 9b) the model tends to produce "secondary" cores that are also documented by measurements of Hoppema et al. (2001). The layer of high concentration further downslope as present in all available measurements is not reproduced by the model. This is further evidence for the model not sufficiently ventilating the abyss. Nevertheless, the model is able to capture the general tracer distribution across the central Weddell Sea: high subsurface concentrations at the continental slopes, in the east an outreaching but too shallow branch of elevated concentration, and a minimum beneath the mixed layer.
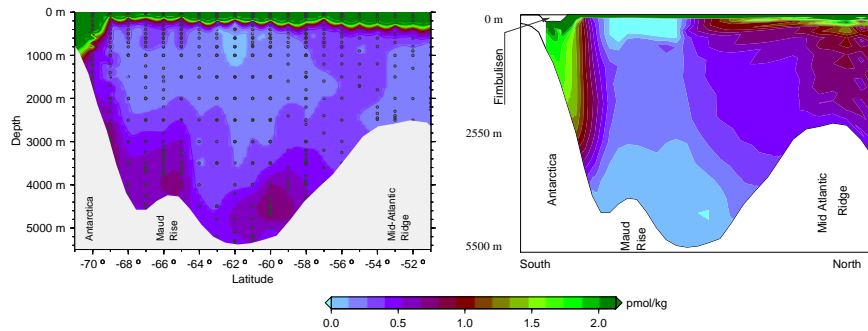
5.2   Section along Greenwich Meridian

Figure 10: CFC11 concentration along the Greenwich Meridian for 1998. a) Observation during *ANT XV/4* and b) simulation. The track is shown in Figure 8. For a better comparison we use for both figures the model topography which includes the northern edge of Fimbulisen Ice Shelf.

The general structure along this section did not change over a period of 14 years (1983-1998) (Klatt et al., 2002), implying limited interannual fluctuations. Again, the high concentrated surface mixed layer is separated from the waters below by a strong concentration gradient (Fig. 10a). Due to wind-induced Ekman pumping, the mixed layer extends to greater depth near the coast. At the continental slope (south), a core exists at about 3000 m, in proximity to increased concentrations on top of Maud Rise. The latter was first detected by the measurements in 1996. Two CFC-features are located at the Mid-Atlantic Ridge (north), a core at the slope's foot in 4000 m depth and a plume of elevated concentrations extending from the surface mixed layer down to the crest of the ridge.

In agreement with observations, the model's mixed layer is separated from the water masses below by a sharp concentration gradient at the center of the gyre (Fig. 10b). However, the simulated concentration minimum does not extend as far north as the observed one. Over the Midatlantic Ridge a "curtain" of high concentrations, attached to the surface mixed layer, extends with slightly decreasing values to great depth. The

14

model does not reproduce the southern core, but for the observed core on the continental slope at about 3000 m the simulated concentrations of 0.6 pmol/kg – 1.0 pmol/kg agree with the measured ones of 0.8 pmol/kg. The second maximum on top of Maud Rise is missing, although the model shows slightly higher concentrations to the east of this section. Above the Mid-Atlantic Ridge, simulated concentrations are too high mainly due to the disintegration of the strong gradient between surface mixed layer and deep ocean and of a too shallow stratification of tracer-carrying water masses (see below). Furthermore, the maximum at the slope does not exist and the simulated concentration (0.3 pmol/kg) is much lower than the observed one (0.7 pmol/kg).

5.3   Discussion of the two cross sections

While many features, for example, the CFC-saturations and their temporal evolution (Rodehacke et al., 007b) as well as CFC-inventories along the Greenwich Meridian (Section 6.1) agree reasonably well with the observations, the model has obvious deficiencies. Namely, it does not reproduce subsurface cores clearly separated from the surface mixed layer, and the cores are in general too wide, probably due to insufficient horizontal model resolution. Given the small spatial scales of the observed cores (less than $1° – 3°$) on the slope off the Antarctic Peninsula (Hoppema et al., 2001), one cannot expect to find these features in a $1.5° \times 1.5° \cos \phi$ model. It is even surprising that the simulated concentrations along the Greenwich Meridian are that close to the observations of Klatt et al. (2002). In addition, the model does not stratify the inflowing and outflowing freshly ventilated water masses of the Weddell Sea at proper depths. This might be caused by an inappropriate representation of the descent of dense water masses along the continental slope, a point addressed below.

6   CFC-Inventories

As shown in the preceding section, the model does not capture well the vertical structure of the tracer distribution. However, if the modeled freshly ventilated water masses follow the observed spreading paths in top view, inventories, i.e., vertical integrals of tracer concentrations over the whole water column, should agree between measurements and the simulation. For a quantitative analysis, we inspect local inventories and derive the penetration depth along the Greenwich Meridian, interpolating all cross-section observations on a regular grid of $1°$ horizontal resolution. The Greenwich Meridian section allows a sensitive test, since the tracer distribution is well known (Klatt et al., 2002) and it is sufficiently far away from the sources of the cores.

6.1   CFC inventories along the Greenwich Meridian

The local inventories of CFC11 concentration and CFC11 partial pressure are defined as vertical integrals and the penetration depth as the vertical integral divided by the corresponding surface concentration according to Dutay et al. (2002). The properties are calculated for the three cruises *ANT X/4*, *ANT XIII/4*, and *ANT XV/4*, which were carried out around July 1992, May 1996, and April 1998, respectively.

The inventories of the three cruises are quite similar (Fig. 11) with values highest at the southern continental slope and fluctuating around 2.2 mmol m^{-2} further to the north. The band of slightly higher concentrations above the Mid-Atlantic Ridge (Fig. 10a, latitude range 54°–57° S) is not captured by the local inventories because they are strongly determined by the surface mixed layer concentration. The meridional distribution of the partial pressure is almost identical (not shown). With time the penetration depth of all observations increases due to increasing inventories, which highlights the ongoing deep ventilation.

The simulated inventories and deduced penetration depths increase with time for the flux boundary condition (Eq. 1) as well as for the sensitivity study, in which the surface concentration was held at the equilibrium concentration, i.e., the surface layer is saturated by 100% at every time step. The increasing penetration depths in time are more pronounced in the simulations than in the observations. The preferred spreading paths across the Greenwich Meridian within the model can be inferred from the local maxima of all properties at the Antarctic continental slope and above the Mid-Atlantic Ridge. In between, a local minimum exists indicating that only a limited portion of tracer-enriched water masses penetrates into the center of the Weddell Gyre.

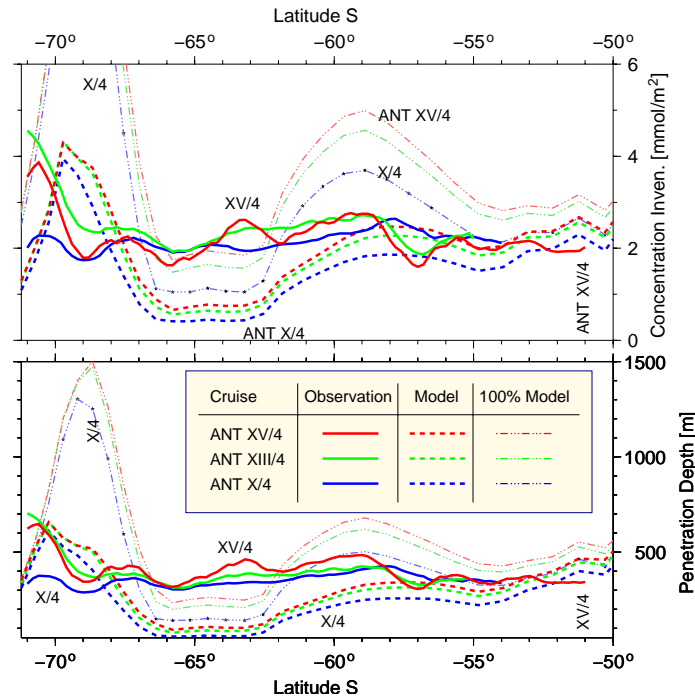Figure 11: Inventories of CFC-11 concentration (upper), and CFC-11 penetration depth (lower) versus latitude. Observations are marked as solid lines. Model results using the flux boundary condition (Eq. 1) marked as (tiny) dashed lines and model results using a saturated ocean surface layer at every time step as dashed-dotted lines. The different cruises are color and symbol coded, as indicated in the legend.

16

Modeled and observed concentration inventories and the penetration depths all have a local maximum at the Antarctic coast. The model's slight northern shift is caused by the coarser and smoothed bottom topography which puts model grid points south of 70°S below the edge of the Ekström/Fimbulisen Ice Shelf. Hence, these grid points of the uppermost layer are located below the ice shelf in 150 m depth, while for the observations the southernmost surface mixed layer still has contact with the atmosphere. The reason for the differences between the wintertime 1992-observation (*ANT X/4*) and the simulation is related to different sea ice conditions. During that year a positive sea ice anomaly led to higher sea ice concentration in the south and a northward extension of the sea ice edge which is not represented by the climatological condition used for our model. This results in a reduced CFC flux across the atmosphere-ocean interface leading to a reduced CFC concentration in the surface mixed layer and, thus, to a reduced CFC inventory at the section's southern end. North of 59 °S, however, simulations and observations coincide.

Along the main spreading paths the penetration depth is well represented and the integrated tracer values of the model agree with the measurements. Since the inventory is strongly influenced by the surface values (Fig. 12), a potential bias between observations and simulation can be recognized by comparing both inventories and penetration depths. For example, a positive surface concentration bias is accompanied by a reduced concentration at depth to get a congruent inventory for observations and simulation. In this case, however, the scaling by the surface-layer concentration will make the penetration depth too small.

The model's lateral diffusion is Reynolds number dependent and, therefore, works predominantly along the flow and less in the cross-flow direction. A more isotropic diffusion would certainly transport more tracers from the local maxima, the main spreading paths, into the center of the gyre. This, however, would destroy the doming of the temperature and salinity fields characteristic for both sections crossing the Weddell Gyre and, thus, would degrade the model's overall skill to simulate quite realistically the Weddell Gyre circulation. In addition, the simulated diffusive tracer transport perpendicular to the main flow occurs mostly at 500–2500 m depth. Consequently, we expect an enhanced lateral diffusion to destroy the observed concentration minimum below the surface mixed layer, increasing the differences between observations and simulation.

An enhanced tracer flux exclusively across the atmosphere-ocean interface would not completely eliminate the local minima, because they even exist in the sensitivity study where the surface saturation was held fixed at 100%. This neglects any sea ice and implies a nearly infinite flux for the case of an undersaturated surface. Instead, the inventories and penetration depths at the location of the observed CFC cores and at the northern end of the section clearly exceed the observed values.

Dutay et al. (2002) compare the results of thirteen CFC-simulations with global ocean circulation models with observations along two sections in the Atlantic (AJAX) and Pacific Oceans (WOCE-P15s), and in the bottom layer of the Southern Ocean (Orsi et al., 1999). The *AJAX* section within the Weddell Sea, conducted in 1983, is identical to the *ANT XV/4* section. None of the models is able to simulate the sharp transition between the surface mixed layer and the waters below nor the cores of freshly ventilated water masses at the Greenwich Meridian. In contrast, our model reaches at least a qual-

17

itative agreement not achieved by any of the coarse resolution models, for example, the strong concentration gradient separating mixed layer and deeper ocean, and the quite realistic CFC inventories and penetration depths. Even the very high eddy-resolving (0.1°) z-coordinate model (Matsumoto et al., 2004) with 54 vertical layers is unable to resolve the CFC cores along the Greenwich Meridian (Sasai et al., 2004). Since the parameterization of vertical mixing and the representation of downslope flow at the continental margin are crucial for deep and bottom water formation and spreading, the reason for the deficiencies may well lie in the treatment of the bottom boundary layer in these models.

Differences in resolution, the vertical coordinate system, the coupling to a sea ice model as well as choices for the numerical algorithm and parameterization all have to be considered when comparing ocean circulation models. We note that none of the models (Dutay et al., 2002; Doney and Hecht, 2001) achieve a sufficient agreement between observed and simulated spreading paths within the Southern Ocean. Only the results of Sasai et al. (2004) come close to the observations, although they restored hydrographic variables to monthly mean climatological values throughout the water column in parts of the Weddell and Ross Seas. In contrast, our results agree apparently better with the observations of Orsi et al. (1999) with no restoring except near the northern boundary.

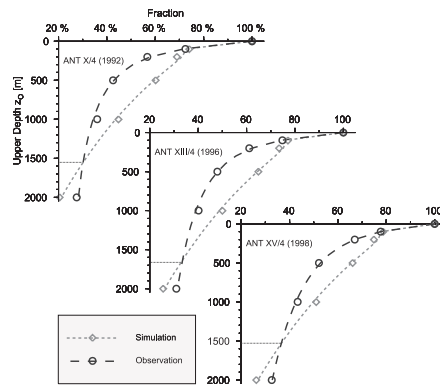## 6.2   Depth dependency of the CFC-inventories

Figure 12: Depth dependence of the tracer inventory for the upper 2000 m of the water column calculated for three cruises (years) along the Greenwich Meridian (see labels). The points are connected by interpolated curves. Red lines indicate the level where the simulation starts to show a deficit in the tracer inventory for greater depth. By definition (Eq. 2) both curves are congruent 100% at $z_0 = 0$.

For the inventories along the Greenwich Meridian, the tracers were integrated from the bottom to the surface using gridded data. To obtain a fractional CFC content versus depth we first calculated the inventories over the whole latitudinal range (entire section) from the bottom to a variable depth z_0. For our analysis we choose z_0 to be 2000 m,

1000 m, 500 m, 200 m, 100 m, and 0 m (Tab. 1). The latter depth yields the total tracer concentration of the whole section because z_0 is equal to the ocean surface. That value was then used to scale the inventories for the other z_0, i.e., the fractional tracer inventory below depth z_0 was obtained from:

$$\frac{\int_{\phi_{\mathrm{s}}}^{\phi_{\mathrm{n}}} \int_{z_{\mathrm{b}}(\phi)}^{\mathbf{z_0}} c(\phi', z')dz' \, d\phi'}{\int_{\phi_{\mathrm{s}}}^{\phi_{\mathrm{n}}} \int_{z_{\mathrm{b}}(\phi)}^{\mathbf{z=0}} c(\phi', z')dz' \, d\phi'} \cdot 100[\%], \qquad (2)$$

with ϕ_{n} and ϕ_{s} representing the northern and southern boundary, respectively, and $z_{\mathrm{b}}(\phi)$ the bottom depth at latitude ϕ. The depth-dependent fractional inventories are by definition 100% at the ocean surface, decreasing monotonically to 0% at the ocean floor (z_b). Since we scale the depth-dependent inventory with the total inventory, any errors in the solubility function or differences in the choice of parameters, which control the CFC uptake between different realizations, are canceled out.

This procedure allows one to determine the depth range in which tracer-enriched water masses tend to spread. We restrict our comparison, however, on the fractional concentration inventories of the upper 2000 m, because the model overestimates sub-surface concentrations on the expense of the concentrations at greater depth. Between the points the curves are approximated such that the maximum difference between approximated values and data points is less than 1% and never exceeds 2.1%. While the curves representing the observations decline about exponentially with depth, the simulated curves can be described as a combination of two linear segments due to the strong gradient between the surface mixed layer and the deep ocean (Fig. 12).

At the surface the values are by definition identical 100% and remain close for the upper 100 m, diminishing within this depth interval by 21.3–26% (observations) and 22.3–27.6% (simulation). This shows the above mentioned strong influence of the surface mixed layer concentration on the water column inventory. Down to ∼1580 m the simulated fractions are up to 18% higher than the observed ones, but the relation changes sign for greater depths. The fraction of the tracer concentration below 2000 m amounts to 27–33% for the observations and 20–26% for the simulation. This means that more than 27% (20%) of the observed (simulated) tracer concentrations are placed below 2000 m. Thus, the deep tracer content is almost identical to the content of the upper 100 m. The fractional content at great depth increases with time (see values at 2000 m in Fig. 12), because the freshly ventilated water masses, formed at a time of increasing atmospheric CFC concentrations, have a transit time of several years from the formation sites to the Greenwich Meridian (13.5±2.5 years for the northern core (Klatt et al., 2002)). In addition, increasing saturations at the deep and bottom water formation sites (Rodehacke et al., 007b) cause increasing concentrations in newly formed water masses even for stagnating atmospheric CFC partial pressures.

The fractional inventories clearly show that the model places tracer-enriched, freshly ventilated water masses too shallow in the water column. The fractional differences are highest at about 400 m depth (Fig. 12). If we allow a difference of 5% between simulated and observed fractional concentrations, the tracer concentration missing at great depth is placed in the model's 150–1200 m depth range.

19

6.3 Discussion of the tracer inventories along the Greenwich Meridian

Based on the spreading paths in the bottom layer (Fig. 8), the section across the central Weddell Sea (Fig. 9), and three independent observations along the Greenwich Meridian (Fig. 10) the model seems to reproduce reasonable well the horizontal spreading paths of CFC-enriched water masses. However, the model obviously does not transfer these water masses to the proper depth ranges as the detailed analysis along the Greenwich Meridian shows. The transect-wide integrated tracer concentration inventory and its fractional inventory against depth indicate that the tracer-enriched waters missing in the deep ocean are instead to be found at 150–1200 m depth. Since the Greenwich Meridian section is far away from the formation sites (Prydz Bay for the southern core and western Weddell Sea for the northern core), it is unlikely that the tracer carrying water masses will further descend; a result typical for this model. Like for many other models with this resolution (e.g., Fichefet and Goosse (1999); Doney and Hecht (2001); Dutay et al. (2002)), the downslope flow of dense water masses remains to be a challenge even for models using terrain-following coordinates (Griffies et al., 2000; Willebrand et al., 2001).

Table 1: Depth dependency of the CFC inventory along the Greenwich Meridian. 'Inv' specifies the total concentration inventory of the section between the bottom and the upper boundary z_0. The fraction [%] of the total inventory in the depth range between the bottom and z_0 is given by 'Ratio'.

Cruise (Year)	Limit z_0 [m]	Observation Inv. $[\frac{mol}{m}]$	Observation Ratio [%]	Simulation Inv. $[\frac{mol}{m}]$	Simulation Ratio [%]
ANT X/4	0	4.11	100	3.64	100
(1992)	100	2.98	72.4	2.70	74.0
	200	2.33	56.7	2.51	68.9
	500	1.75	42.5	2.19	60.2
	1000	1.48	36.0	1.63	44.8
	2000	1.13	27.5	0.74	20.5
ANT XIII/4	0	4.48	100	3.39	100
(1996)	100	3.35	74.7	2.61	77.1
	200	2.74	61.1	2.48	73.4
	500	2.14	47.9	2.20	64.9
	1000	1.80	40.1	1.69	50.0
	2000	1.38	30.9	0.86	25.5
ANT XV/4	0	5.01	100	3.86	100
(1998)	100	3.89	77.7	3.04	78.7
	200	3.35	67.0	2.89	74.9
	500	2.61	52.1	2.55	66.0
	1000	2.17	43.3	1.97	51.0
	2000	1.64	32.6	1.01	26.2

7 Flow from the Weddell Sea into the South Scotia Sea

Newly formed deep and bottom waters that flow northward along the Antarctic Peninsula leave in part the Weddell Sea through gaps in the South Scotia Ridge (Schodlok et al., 2002) to spread into the South Scotia Sea (Fig. 8). Observed and simulated CFC profiles combined with the above discussed sections and the spreading in the bottom layer highlight the paths of these freshly ventilated water masses. This also allows us to evaluate whether the missing deep core at the Mid-Atlantic Ridge is related to an export out of the Weddell-Enderby Basin before the newly formed water masses reach the Greenwich Meridian.

The observed and simulated CFC concentrations are highest in the surface mixed layer, due to contact with the atmosphere, and in general decrease with depth (Fig. 13). The profiles near South Georgia (#1; numbers in brackets correspond to numbers on the map indicating location of the profiles) and in Drake Passage (#6 and #7) reveal that the surface signal almost vanishes below 1000 m (Roether et al., 1993). In contrast, the measured profiles north of South Orkney Islands (#4 and #5) show an increase with depth close to the bottom as all profiles in the Scotia Sea do, though the gradient is not that pronounced. These local CFC maxima in the bottom layer reflect the spreading of freshly ventilated waters of Weddell Sea origin (Beining, 1993; Klatt, 2002). The latter is also confirmed by hydrographic observations of Fahrbach et al. (2001). The model does not reproduce the observed high-concentrationed bottom layer (see discussion in Section 6.2), however, the bottom concentration in the northeastern Scotia Sea between South Georgia and the South Sandwich Islands (#1–#3) indicates that this region is ventilated by waters of Weddell Sea origin, though with lower intensity. These water masses flow north toward the Argentine Basin as suggested by Naveira Garabato et al. (2002) and Schodlok et al. (2002).

In the center of Drake Passage the penetration of high-concentrated water masses to 750 m depth is related to a local temperature minimum between two fronts, which both have the characteristic of the Polar Front (Roether et al., 1993). Since the model does not resolve the frontal systems, this feature is absent in the simulation. Similar to the observations (Roether et al., 1993) the model shows elevated concentrations in southern Drake Passage (#6). They are slightly higher than observed, but they would not be noticed, if we would have used for greater depths the same horizontal scaling as for the upper 1000 m. Since the model underestimates the concentrations in the bottom layer, in particular, near the South Orkney Islands (#5), it is suggested that a major fraction of the freshly ventilated bottom water flows westward through Drake Passage instead into the South Scotia Sea. However, the model does not resolve properly the Powell Basin, and Bransfield Strait is absent because the South Shetland Islands are not included. Such topographic features might hamper the flow of Weddell Sea deep waters to the west and reduce the simulated CFC concentrations west of the Antarctic Peninsula, which are ≈ 0.5 pmol/kg for model year 1992 but only ≤ 0.03 pmol/kg for the corresponding observation (eastern WOCE line S4P in March, 1992; not shown). Simulations with enhanced resolution in the Weddell Sea (Schodlok et al., 2002) support our assumption that the exaggerated westward flow is related to the too coarse model resolution. However, this does not explain the missing northern core at the Greenwich Meridian because the export in the northwestern Weddell Sea is compensated by a re-
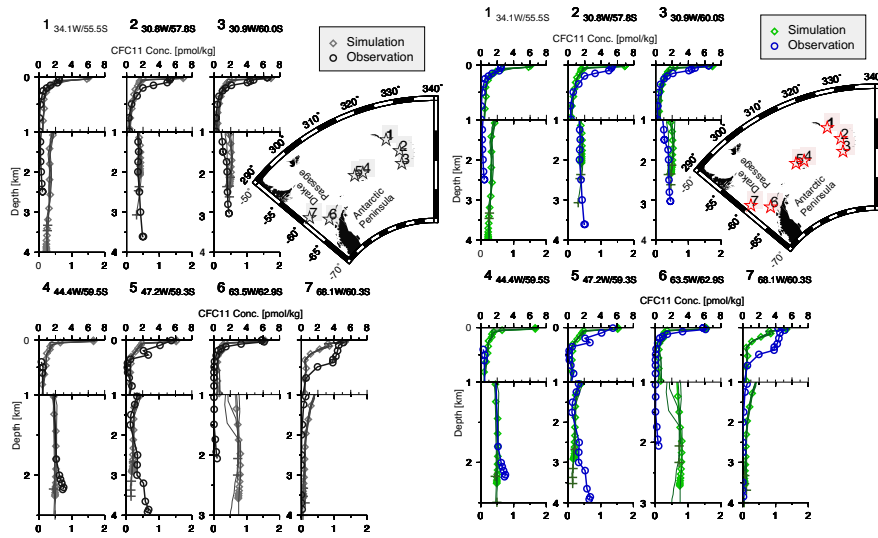
Figure 13: CFC11 concentration profiles in the Scotia Sea (inset). The profiles originate from cruises *JCR 10, 1995* (profile 1–3), *ANT XV/4, 1998* (5), and *M11/4, 1990* (4 and 6–7). The blue circles indicate measurements while the green diamonds represent model results. Modeled profiles of neighboring grid points are shown as thin green lines and its maximum depth is marked by dark green crosses. Note the different scaling of both x-axes at 1000 m and the nonuniform depths of all profiles. The geographical positions are indicated as small numbers below the profile number which corresponds to the numbers on the map (inset).

duced outflow further downstream, for example, near the Southern Orkneys (#4, #5). In addition, a core exists east of the Southern Orkney Islands at a depth too shallow, but the simulated concentration agrees reasonably with the observed one.

The simulated total CFC inventory as well as the penetration depths both agree reasonably with the observations at the Greenwich Meridian. Therefore, the outflow of freshly ventilated water across the South Scotia Ridge, cannot be the reason for the absence of the deep core at the Mid-Atlantic Ridge.

8   Conclusions

Our regional CFC simulation highlights the spreading of newly ventilated water masses formed around Antarctica. In agreement with observations, the model reproduces the main deep and bottom water formation sites in the Ross Sea, Prydz Bay, and the southwestern Weddell Sea. The Ross Sea ventilates the Southeast Pacific Basin as well as the Antarctic Coastal Current and thus contributes to the ventilation of the Australian-Antarctic Basin. Prydz Bay adds tracer-enriched water to the coastal current and therefore represents the eastern source of newly formed water masses entering the Weddell Sea. Here, strong sources are located at the southwestern continental slope which feed the deep cores in the Weddell-Enderby Basin and the South Scotia Sea with young waters, carrying high tracer concentrations. In the simulation, minor formation sites exist off Adélie Coast and in front of Wilkes Land.

An interesting perception of this study, which results, in particular for the Weddell Sea, from the combination of tracer observations and current measurements (Fahrbach et al., 1994), is the coincidence between the cores of high concentrations and high velocities. Our model reproduces at several places elevated concentrations that correspond to the depth of the observed cores. However, a detailed analysis shows that the spreading levels of the freshly ventilated water masses are too shallow. The tracers that are missing in the deep ocean are found in a depth range of 150–1200 m.

The model's inability to reproduce the core of high CFC concentration at the Mid-Atlantic Ridge near to the Greenwich Meridian cannot be attributed to an upstream northward export of CFC-enriched waters from the Weddell Sea for several reasons. The slightly too concentrated flow through the southern Drake Passage is compensated by a lower concentrationed bottom layer in the Scotia Sea (Section 7). The combined results of tracer inventory and penetration depth along the Greenwich Meridian show that enough tracer-enriched water exists at both ends of the section (Section 6, Fig. 11). This would not be the case if too much tracer-enriched water would leave the Weddell Sea before reaching the Greenwich Meridian. The depth-dependent section-integrated inventory along Greenwich Meridian clearly indicates that the tracers are placed too shallow (Fig. 12). Similarly, the section across the central Weddell Sea shows at the eastern end a too shallow inflow of high-concentrated deep water from eastern sources (Fig. 9) as well as at the western end a less concentrated bottom water in proximity to the formation sites. Therefore, the comparison between observations and model results suggests that an improper vertical penetration of high concentrated water is one reason, besides the too coarse model resolution, for the missing northern core.

Our model results are more realistic than those of other models of similar resolu-

23

tion, but it is obvious that an appropriate representation of downslope flow of dense water masses in coarse resolution models still needs to be developed. Even a drastic increase in resolution does not solve the problem as the results of the eddy-resolving ($0.1°$), 54 layer z-coordinate model of Sasai et al. (2004) indicate. For long-term simulations of a "complete" earth system model, which address, for example, questions of climate variability and change, the glacial cycle, or the storage of CO_2 in the ocean, an appropriate formulation of deep and bottom water formation is essential. Tracer simulations like the present one are an excellent tool to demonstrate success or identify deficiencies of a given model or method.

References

Asher, W. and R. Wanninkhof (1998). Transient tracers and air-sea gas transfer. *Journal of Geophysical Research 103*(C8), 15939–15958.

Baines, P. and S. Condie (1998). Obervations and modelling of Antarctic downslope flows: A review. In S. Jacobs and R. Weiss (Eds.), *Ocean, Ice and Atmosphere: Interaction at the Antarctic Continental Margin*, Volume 75 of *Antarctic Research Series*, 29–49. American Geophysical Union.

Beckmann, A., H. Hellmer, and R. Timmermann (1999). A numerical model of the Weddell Sea: Large scale circulation and water mass distribution. *Journal of Geophysical Research 104*(C10), 23375–23391.

Beining, P. (1993). *Darstellung und Interpretation ozeanischer FCKW-Verteilungen*. Disseration, Universität Bremen.

Carmack, E. and T. Foster (1975). Circulation and distribution of oceanographic properties near the Filchner Ice Shelf. *Deep-Sea Research 22*, 77–90.

Doney, S. and M. Hecht (2001). Antarctic Bottom Water formation and deep water chlorofluorocarbon distributions in a Global Ocean Climate Model. *Journal of Physical Oceanography 32*(6), 1642–1666.

Doney, S. and W. Jenkins (1988). The effect of boundary conditions on tracer estimates of thermocline ventilation rates. *Journal of Marine Research 46*, 947–965.

Dutay, J.-C., J. Bullister, S. Doney, J. Orr, R. Najjar, K. Caldeira, J.-M. Campin, H. Drange, M. Follows, Y. Gao, N. Gruber, M. Hecht, A. Ishida, F. Joos, K. Lindsay, G. Madec, E. Maier-Reimer, J. Marschall, R. Matear, P. Monfray, A. Mouchet,

G.-K. Plattner, J. Sarmiento, R. Schlitzer, R. Slater, I. Totterdell, M. Weirig, Y. Yamanaka, and A. Yool (2002). Evaluation of ocean model ventilation with CFC-11: comparison of 13 global ocean models. *Ocean Modelling 4*, 89–120.

England, M. H., V. Garcon, and J.-F. Minster (1994). Chlorofluorocarbon uptake in a world ocean model 1. Sensitivity to the surface gas forcing. *Journal of Geophysical Research 99*(C12), 25215–25233.

Fahrbach, E. (1993). Zirkulation und wassermassenbildung im weddellmeer. *Die Geowissenschaften 7*, 246–253.

Fahrbach, E., S. Harms, G. Rohardt, M. Schröder, and R. Woodgate (2001, 02). Flow of bottom water in the northernwestern Weddell Sea. *Journal of Geophysical Research 106*(C2), 2761–2778.

Fahrbach, E., M. Knoche, and G. Rohardt (1991). An estimate of water mass transformation in the southern Weddell Sea. *Mar.Chem. 35*, 25–44.

Fahrbach, E., G. Rohardt, N. Scheele, M. Schröder, V. Strass, and A. Wisotzki (1995). Formation and discharge of deep and bottom water in the northwestern Weddell Sea. *Journal of Marine Research 53*, 515–538.

Fahrbach, E., G. Rohardt, M. Schröder, and V. Strass (1994). Transport and structure of the Weddell Gyre. *Annales Geophysicae 12*, 840–855.

Fichefet, T. and H. Goosse (1999). A numerical investigation of the spring ross sea polyna. *Geophysical Research Letters 26*(8), 1015–1018.

Foldvik, A., T. Gammelsrød, and T. Tørrensen (1985a). Hydrographic observations from the Weddell Sea during the Norwegian Antarctic Research Expedition 1976/77. *Polar Research 3*, 177–193.

Foldvik, A., T. Gammelsrød, and T. Tørrensen (1985b). Physical oceanography studies in the Weddell Sea during the Norwegian Antarctic Research Expedition 1978/79. *Polar Research 3*, 195–207.

Foster, T. and E. Carmack (1976). Frontal zone mixing and Antarctic Bottom Water formation in the southern Weddell Sea. *Deep-Sea Research 23*, 301–317.

Foster, T. and E. Carmack (1977). Antarctic bottom water formation in the Weddell Sea. In M. Dunbar (Hrsg.), *Polar Oceans*, 167–177. Calgary: Arctic Institute of North America.

Foster, T., A. Foldvik, and J. Middleton (1987). Mixing and bottom water formation in the shelf break region of the southern Weddell Sea. *Deep-Sea Research 34*(11), 1771–1794.

Gloersen, P., W. Campbell, D. Cavalieri, J. Comiso, C. Parkinson, and H. Zwally (1992). Arctic and Antarctic Sea Ice 1978–1987: Satellite Passive-Microwave Observations and Analysis. NASA Special Publication SP-511, NASA, Washington, DC.

Gordon, A. (1998). Western Weddell Sea Thermohaline Stratification. In S. Jacobs and R. Weiss (Eds.), *Ocean, Ice and Atmosphere: Interaction at the Antarctic continental margin*, Volume 75 of *Antarctic Research Series*, 215–240. American Geophysical Union.

Griffies, M., C. Böning, F. Bryan, E. Chassignet, R. Gerdes, H. Hasumi, A. Hirst, A.-M. Treguier, and D. Webb (2000). Developments in ocean climate modelling. *Ocean Modelling 2*, 123–192.

Haidvogel, D. B., J. L. Wilkin, and R. Young (1991). A semi-spectral primitive equation ocean circulation model using vertical sigma and orthogonal curvilinear horizontal coordinates. *Journal of Computational Physics 94*(1), 151–185.

Haine, T. and K. Richards (1995). The influence of the seasonal mixed layer on oceanic uptake of CFCs. *Journal of Geophysical Research 100*(C6), 10727–10744.

Hellmer, H. (2004). Impact of Antarctic ice shelf melting on sea ice and deep ocean properties. *Geophysical Research Letters 31*(10), 28–29. L1037 DOI:10.1029/2004GL019506.

Hoppema, M., O. Klatt, W. Roether, E. Fahrbach, K. Bulsiewicz, C. Rodehacke, and G. Rohardt (2001). Prominent renewal of Weddell Sea Deep Water from remote source. *Journal of Marine Research 59*, 257–279.

Huhn, O., M. Rhein, W. Roether, C. Rodehacke, M. Schroeder, and M. Schodlok (2006). Tracer observations in the western Weddell Sea from the 90th: Contributions of the Ice Shelf Water to the formation of Weddell Sea Deep and Bottom Water. *Deep-Sea Research x*(x), 13. submitted.

Klatt, O. (2002). *Interpretation von FCKW-Datensätzen im Weddellmeer*. Disseration, Universität Bremen.

Klatt, O., W. Roether, M. Hoppema, K. Bulsiewicz, U. Fleischmann, C. Rodehacke, E. Fahrbach, R. Weiss, and J. Bullister (2002). Repeated CFC sections at the Greenwich Meridian in the Weddell Sea. *Journal of Geophysical Research 107*(C4), 43. doi: 10.1029/2000JC000731.

Matsumoto, Y., H. Sasaki, T. Kagimoto, N. Komori, A. Ishida, Y. Sasai, T. Miyama, T. Motoi1, H. Mitsudera, H. Takahashi, K.and Sakuma, and T. Yamagata (2004). A Fifty-Year Eddy-Resolving Simulation of the World Ocean: Preliminary Outcomes of OFES (OGCM for the Earth Simulator). *Journal of the Earth Simulator 1*, 35–56.

Mensch, M., W. Smethie Jr, P. Schlosser, R. Weppernig, and R. Bayer (2000). Transient tracer observations during the drift and recovery of Ice Station Weddell. In S. Jacobs and R. Weiss (Eds.), *Ocean, Ice and Atmosphere: Interaction at the Antarctic continental margin*, Volume 75 of *Antarctic Research Series*, 241–256. American Geophysical Union.

Miranda, A., B. Barnier, and W. K. Dewar (1999). Mode waters and subduction rates in a high-resolution South Atlantic simultion. *Journal of Marine Research 57*(2), 213–244.

Muench, R., J. Morison, L. Padman, D. Martinson, P. Schlosser, B. Huber, and R. Hohmann (2001, 2). Maud Rise revisited. *Journal of Geophysical Research 106*(C2), 2423–2440.

Naveira Garabato, A., K. Heywood, and D. Stevens (2002, Aug.). Modification and pathways of Southern Ocean Deep Waters in the Scotia Sea. *Deep-Sea Research 49*(4), 681–705.

Olbers, D., V. Gouretski, G. Seiß, and J. Schröter (1992). Hydrographic Atlas of the Southern Ocean. Technical report, Alfred-Wegener-Institut for Polar and Marine Science, Bremerhaven, Germany.

Orsi, A., G. Johnson, and J. Bullister (1999). Circulation, mixing, and production of Antarctic Bottom Water. *Progress in Oceanography 43*, 55–109.

Rodehacke, C. B., H. H. Hellmer, , W. Roether, and T. Hall (2007b). Temporal evolution of CFC11 and CFC12 saturations in the Antarctic Marginal Seas: Ocean circulation model results. *XXXX ??* in preparation.

Rodehacke, C. B., H. H. Hellmer, O. Huhn, and A. Beckmann (2006a). Ocean/ice shelf interaction in the southern Weddell Sea: Results of a regional numerical helium/neon simulation. *Ocean Dynamics*, 1–11. doi: 10.1007/s10236-006-0073-2.

Roether, W., R. Schlitzer, A. Putzka, P. Beining, K. Bulsiewicz, G. Rohardt, and F. Delahoyde (1993). A chlorofluoromethane and hydrographic section across Drake Passage: Deep Water ventilation and meridional property transport. *Journal of Geophysical Research 98*(C8), 14423–14435.

Sasai, Y., A. Ishida, Y. Yamanaka, and H. Sasaki (2004). Chlorofluorocarbons in a global ocean eddy-resolving OGCM: Pathways and formation of Antarctic Bottom Water. *Geophysical Research Letters 31*(L12305), 4. doi: 10.1029/2004GL019895.

Schodlok, M., H. Hellmer, and A. Beckmann (2002). On the transport, variability and origin of dense water masses crossing the South Scotia Ridge. *Deep Sea Research II 49*(21), 4807–4825.

Schodlok, M., C. Rodehacke, H. Hellmer, and A. Beckmann (2001). On the origin of the deep CFC maximum in the eastern Weddell Sea — numerical model results. *Geophysical Research Letters 28*(14), 2859–2862.

Schröder, M. and E. Fahrbach (1999). On the structure and the transport of the eastern Weddell Gyre. *Deep-Sea Research 46*(2), 501–527.

Talley, L. (1996). Antarctic Intermediate Water in the Southern Atlantic. In G. Wefer, W. Berger, G. Siedler, and D. Weeb (Eds.), *The South Atlantic: Present and past circulation*, 219–238. Berlin, Heidelberg: Springer-Verlag.

Talley, L. (1999). Some aspects of ocean heat transport by the shallow, intermediate and deep overturning circulations. In P. Clark, R. Webb, and L. Keigwin (Eds.), *Mechanisms of global climate change at millenial time scales*, 1–22. American Geophysical Union.

Timmermann, R. and A. Beckmann (2004). Parameterization of vertical mixing in the Weddell Sea. *Ocean Modelling 6*, 83–100.

Walker, S., R. Weiss, and P. Salameh (2000). Reconstructed histories of the annual mean atmospheric mole fractions for the halocarbons CFC-11, CFC-12, CFC-113, and carbon tetrachloride. *Journal of Geophysical Research 105*(C6), 14285–14296.

Wanninkhof, R. (1992). Relationship between wind speed and gas exchange over the ocean. *Journal of Geophysical Research 97*(C5), 7373–7382.

Warner, M. and R. Weiss (1985). Solubilities of chloroflurocarbons 11 and 12 in water and seawater. *Deep-Sea Research 32*(12), 1485–1497.

Weppernig, R., P. Schlosser, S. Khatiwala, and R. Fairbanks (1996). Isotope data from Ice Station Weddell: Implications for deep water formation in the Weddell Sea. *Journal of Geophysical Research 101*(C10), 25723–25739.

Willebrand, J., B. Barnier, C. Böning, C. Dietrich, P. Killworth, C. Le Provost, Y. Jia, J.-M. Molines, and A. New (2001). Circulation characteristics in three eddy-permitting models of the North Atlantic. *Progess in Oceanography 48*, 123–161.

Zheng, M., W. De Bruyn, and E. Saltzman (1998). Measurements of the diffusion coefficients of CFC-11 and CFC-12 in pure water and seawater. *Journal of Geophysical Research 103*(C1), 1375–1379.